J. Plasma Phys. (2024), *vol*. 90, 905900605
Published by Cambridge University Press

doi:10.1017/S0022377824001399

Kinetic instabilities in two-isotopic plasma in the gas-dynamic trap magnetic mirror

Evgeniy A. Shmigelsky [1,2,3,†], Andrey K. Meyster [1], Ivan S. Chernoshtanov [1,2], Andrej A. Lizunov [1,2], Alexander L. Solomakhin [1,2,3] and Dmitry V. Yakovlev [1]

[1]Budker Institute of Nuclear Physics of Siberian Branch Russian Academy of Sciences, Acad. Lavrentieva Pr. 11, 630090 Novosibirsk, Russia

[2]Novosibirsk State University, Pirogova st. 1, 630090 Novosibirsk, Russia

[3]Federal Research Center A.V. Gaponov-Grekhov Institute of Applied Physics of the Russian Academy of Sciences, Ulyanova st. 46, 603950 Nizhny Novgorod, Russia

(Received 19 August 2024; revised 14 October 2024; accepted 15 October 2024)

A fusion neutron source (FNS) based on the gas-dynamic trap (GDT, Budker Institute, Novosibirsk) is considered for confinement of two-species plasma heated by neutral beam injection in a regime where the fast ion distribution function is far from Maxwellian. Kinetic instabilities are expected to develop in this regime, and in this paper we investigate the ion-cyclotron instability evolving in moderate densities of pure hydrogen and mixed deuterium–hydrogen target plasmas. The properties of the studied unstable mode, such as its azimuthal wavenumbers, propagation direction and its being affected by changes in the bulk plasma density and composition, allow us to identify it as the drift cyclotron loss cone (DCLC) instability. This mode scatters fast ions and thereby leads to drops in diamagnetic flux signals and increases longitudinal energy and particle losses, with the average energy of the lost ions estimated to be far above the temperature of warm Maxwellian ions. Our interpretation is that the unstable wave grows due to interaction with the fast ions located near the loss cone in the velocity space and scatters them. Applying the method of suppressing the DCLC instability by filling the loss cone with warm plasma, we have determined the values of plasma density and deuterium percentage that allow us to suppress the DCLC instability in the GDT. These findings justify using mixed bulk plasmas in fusion neutron source operation.

Key words: fusion plasma, plasma instabilities

1. Introduction

Axisymmetric linear magnetic mirror traps with neutral beam injection (NBI) can potentially become the basis for a volumetric fusion neutron source (FNS) (Anikeev *et al.* 2015*a*; Bagryansky *et al.* 2020), applicable to the fields of thermonuclear material science

† Email address for correspondence: e.shmigelskii@g.nsu.ru

and to fusion–fission hybrid reactors (Yurov & Prikhod'ko 2014; Yurov & Prikhodko 2016).

The gas-dynamic trap (GDT) in the Budker Institute of Nuclear Physics (Ivanov & Prikhodko 2017) experimentally supports the idea that an axisymmetric linear magnetic mirror trap can be developed into a FNS. In GDT plasmas neutrons are born in D–D reactions between deuterium nuclei originating from NB injection, which is the main plasma heating system of the GDT.

'Fast' or 'sloshing' ions are formed via charge exchange between injected neutral beams and cold dense target plasma ions, confined in the gas-dynamic regime (Mirnov & Riutov 1979). The fast ion energy confinement time is much shorter than their angular scattering time, and their mean free path far exceeds the length of the trap. As a result, their velocity distribution function is far from Maxwellian and possesses a loss cone, i.e. they are confined to the so-called 'kinetic' regime. The sloshing ions have their axial pressure and density profile maxima in the vicinity of two turning points where the magnetic field strength is twice that of in the centre of the trap. These are also the region where the neutron flux peaks, which is useful for designing an FNS (Simonen *et al.* 2010; Ivanov & Prikhodko 2017). However, in kinetic confinement regimes with non-Maxwellian velocity distribution functions, kinetic instabilities tend to develop, enhancing the scattering of sloshing ions into the loss cone. This scattering also smooths out the fast ions axial pressure profile, decreasing the neutron flux at its maxima points, thus decreasing the efficiency of an FNS.

The drift cyclotron loss cone (DCLC) instability (Post 1987) is one of the most likely instabilities to occur under the magnetic mirror trap conditions. The DCLC instability can be considered as a flute-like plasma potential perturbation with a small transverse wavelength, i.e. $k_\perp \rho_i \geqslant 1$ (where $k_\perp$ and ρ_i are the transverse wave vector component and ion gyroradius, respectively), which propagates azimuthally in the ion diamagnetic drift direction. This instability can evolve from drift waves that appear in the presence of a radial plasma density profile gradient inherent to magnetic mirror confinement systems. Drift waves interact with ions and grow in amplitude since the presence of the loss cone and transverse non-uniformity of the plasma create ion velocity distribution functions with regions of positive derivative.

A stability criterion for the DCLC instability can be formulated using the parameter ρ_i/r_{pl}, where r_{pl} is the plasma column radius (Post & Rosenbluth 1966; Kotelnikov, Chernoshtanov & Prikhodko 2017). The threshold value of this parameter is $\rho_i/r_{\mathrm{pl}} \sim 10^{-2}$ if the effects of the limited trap length and the finite relative pressure β are taken into consideration and the low-energy end of the distribution is unpopulated (Tang, Pearlstein & Berk 1972). The value of this parameter in the GDT for fast ions is too high ($0.1 \leqslant \rho_i/r_{\mathrm{pl}} \leqslant 1$), and thus this condition is not fulfilled. Therefore, the GDT plasma is unstable against the DCLC mode in the fully kinetic regime. However, the kinetic regime is considered to be more reasonable for implementation in FNS projects based on the GDT as opposed to the gas-dynamic regime, since the kinetic regime provides longer energy confinement time (Yurov & Prikhodko 2016) and a higher D–T reaction neutron flux (Bagryansky *et al.* 2020).

There are some particular properties of the DCLC instability that allow us to distinguish it from other kinetic instability types. First, the base frequency of the instability is close to the ion cyclotron frequency; the instability can also develop at harmonics of its base frequency. Second, although the assumption $k_\perp \rho_i \geqslant 1$ was used to simplify the dispersion equation, it was shown in several papers (Post & Rosenbluth 1966; Kotelnikov *et al.* 2017) that this condition is valid for the DCLC instability branches with the highest increment values. Thus, an inequality $|m| = |k_\varphi r_{\mathrm{pl}}| \geqslant 1$ for the azimuthal wavenumber m follows

https://doi.org/10.1017/S0022377824001399 Published online by Cambridge University Press

from that condition as well as from the comparability of the ion gyroradius and transverse plasma length. Third, the wave propagates in the direction of the ion diamagnetic drift. These properties were experimentally observed in several mirror devices: 2XII (Simonen 1976), 2XIIB (Turner 1977; Turner, Powers & Simonen 1977), TMX-U (Berzins & Casper 1987), MIX 1 (Koepke *et al.* 1986) and LAMEX (Ferron & Wong 1984). The radial structure of plasma potential perturbations has to be determined by the radial density distribution of warm ions, i.e. ions distributed isotropically in velocity space, which was confirmed in experiments conducted on MIX 1 (Koepke *et al.* 1986) and LAMEX (Ferron & Wong 1984).

The DCLC instability is inherently sensitive to the features of the ion velocity distribution function. Theory predicts that the DCLC instability can be suppressed by partially filling the loss cone with warm ions. The efficiency of this method has been proven in experiments on PR-6 (Kanaev 1979), 2XIIB (Coensgen *et al.* 1975), TMX-U (Berzins & Casper 1987) and MIX 1 (Koepke *et al.* 1986), in which warm ion fractions in plasma, at which the DCLC was stabilised, were evaluated at 5 %–20 %.

As noted in Kotelnikov & Chernoshtanov (2018), there exists a so-called 'spectral rule': the warm ions effectively stabilise the DCLC instability if their cyclotron harmonics coincide with those of the fast ions. The experiments on PR-6 facility (Kanaev 1979) confirmed this by demonstrating that less than 5 % of warm hydrogen was enough to prevent the DCLC instability from forming in hydrogen plasma, while in the case of warm argon its density had to be comparable to the density of the entire plasma.

Implementing a FNS requires use of two-species plasmas (most importantly, D–T plasmas) that are DCLC stable. However, the stabilisation of FNS plasmas by addition of warm ions requires larger amounts of particles compared with single-species plasmas, shifting the plasma away from the kinetic confinement to the gas-dynamic regime and decreasing the output of a neutron source. This issue can be mitigated by using a two-species warm plasma as the target for the neutral beams' capture, so that the first species serves as the necessary fuel component while the second provides the DCLC stabilisation.

In order to test this stabilisation technique we conducted experiments where the hot ion population comprised deuterium and the warm ion population hydrogen. In these circumstances, the cyclotron harmonics of warm ions would only overlap with the even deuterium harmonics, so the DCLC instability was expected to form at odd deuterium harmonics, primarily at the first one. The instability was expected to be completely suppressed when a certain amount of warm deuterium ions was added.

The objectives for this study were to:

(i) identify instability types by their properties;
(ii) suppress the instability in the GDT by using a two-species target plasma (in our case, D–H);
(iii) determine the ratio of isotope densities in the mixture at which the plasma is DCLC stable.

The paper is organised as follows. Section 2 provides a brief description of the GDT, employed diagnostics and signal processing methods as well as a detailed description of the experimental routine and the method used for preparing target plasma and controlling its isotopic composition. Section 3 contains the results obtained on several qualitatively different ion-cyclotron instabilities, one of which we attributed to the DCLC type, the experimentally determined ratio of deuterium to hydrogen in a mixed target which suppresses the DCLC instability and measurements of additional longitudinal energy

https://doi.org/10.1017/S0022377824001399 Published online by Cambridge University Press

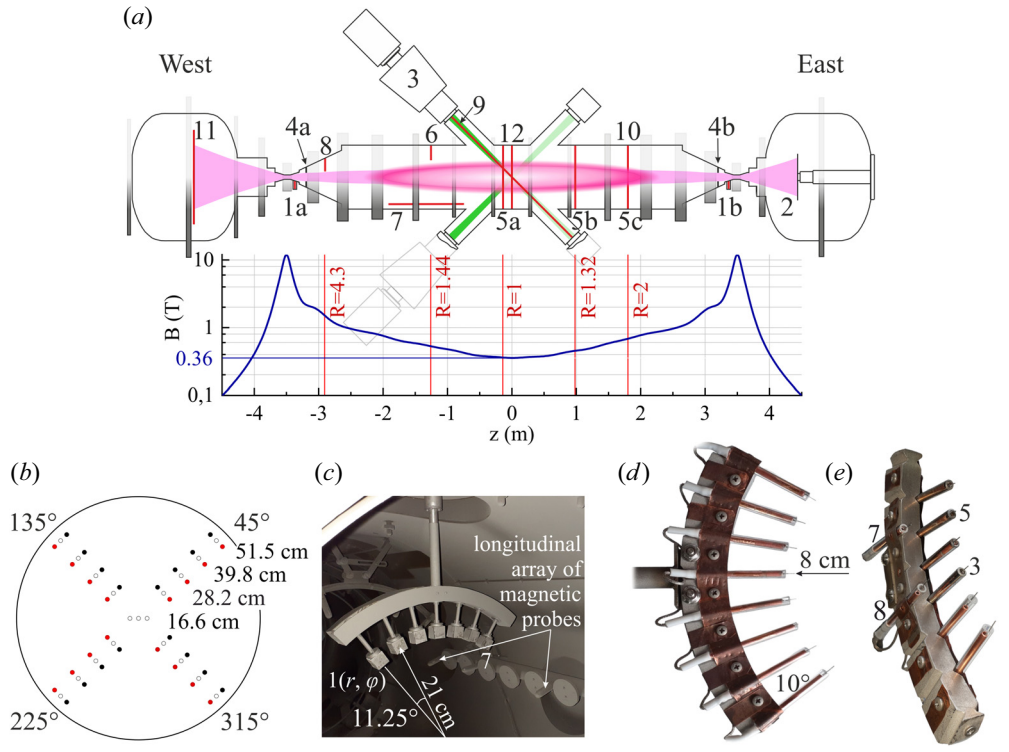

FIGURE 1. (*a*) Scheme of the GDT and its axial magnetic field profile: 1a, 1b – pulsed gas valves; 2 – arc discharge plasma generator; 3 – NB injectors; 4a, 4b – limiters; 5a, 5b, 5c – diamagnetic loops; 6 – azimuthal array of the magnetic probes; 7 – longitudinal array of the magnetic probes; 8 – azimuthal array of the electrostatic probes; 9 – dispersion interferometer's line of sight (LOS); 10 – spectrometer's LOS plane; 11 – diagnostic plasma absorber; 12 – LOS plane of the Thomson scattering diagnostic; (*b*) layout of the particle and energy flux diagnostics on the western absorber plate (not to scale); black circles mark the pyroelectric bolometers, red circles – the ion current probes; (*c*) photo of the azimuthal array of seven magnetic probes and a longitudinal array of the magnetic probes; (*d*) azimuthal array of electrostatic probes; (*e*) arrangement of the probes for radial correlation measurement.

losses due to the instability with estimates of energy lost per ion. The findings of the study are concluded in § 4.

2. Description of the experiment

2.1. *The GDT device*

The GDT is an axisymmetric magnetic mirror device. The GDT (figure 1*a*) consists of a central solenoid with two magnetic mirror coils at its ends, with the maximum mirror ratio of $R_{max} = B_{max}/B_{min} = 34$. The plasma heating system consists of 8 NBIs with 24 keV deuterium beams inclined at 45° to the GDT axis, supplying up to 5 MW of power in total. A comprehensive description of the GDT facility is provided in Ivanov & Prikhodko (2017).

The experimental routine proceeded as follows. The gas valves were opened in advance and the vacuum vessel was filled with the prepared gas mixture; the valves were closed at the '0' ms moment of the experimental routine. The arc plasma generator in the eastern

https://doi.org/10.1017/S0022377824001399 Published online by Cambridge University Press

expander tank fired from 0.4 to 4.2 ms and produced a plasma with a temperature of a few eV, which then passed through the magnetic mirror and together with the gas comprised a cold dense plasma. This plasma served as a target for neutral deuterium beams injected from 3.8 to 8.6 ms; the charge exchange between target plasma ions and neutral beams resulted in formation of the fast deuteron population. The trapped NBI power was kept approximately constant throughout the experimental campaign ($\approx$1.8 MW). At 4.4 ms electric potential was applied to the limiters to stabilise magnetohydrodynamic (MHD) instabilities during discharge via the 'vortex confinement' method (Beklemishev *et al.* 2010; Bagryansky *et al.* 2011).

Two different plasma components formed in the GDT during the discharge. The first was the warm dense plasma with the Maxwellian velocity distribution. This component, consisting of both ions and electrons, was confined in the gas-dynamic regime (Mirnov & Riutov 1979) due to its high collision frequency. The second component was the fast anisotropic ion population with an essentially non-equilibrium velocity space distribution, similar to the velocity distribution of the injected beams. This property arises from the fact that the fast ion energy confinement time, determined by the ion–electron collisions, is much shorter than their angular scattering time. The fast ion motion is governed by conservation of the magnetic moment and energy; as the result, fast ions move in the region between the points where the local mirror ratio $R = B/B_{\min} = 2$, i.e. the turning points, where their axial density profile peaks.

The diamagnetic pressure (mostly exerted by fast ions) was measured using three diamagnetic loops (figure 1*a*). One of the loops was located at the GDT centre and the other two were at the positions with the values of the $R = 1.32$ and $R = 2$. Magnetic field perturbations were registered by azimuthal and longitudinal magnetic probe arrays. Electric potential perturbations were measured with an azimuthal array of electrostatic probes. The dispersion interferometer (Lvovskiy & Solomakhin 2011) was used to measure the linear electron density along the LOS passing through the trap axis in its central plane. The Thomson scattering diagnostic (Lizunov *et al.* 2023) was used to record electron density and temperature at several points along the radius in the central plane. Additionally, the particle and energy flux measurement system, located on the western plasma absorber, was used to measure longitudinal energy and particles fluxes (figure 1*b*). The system consisted of 16 sets of probes, each set containing a pyroelectric bolometer and an ion current probe (individual probe designs are described in Soldatkina *et al.* 2020).

2.2. *Magnetic probes*

The spatial structure of the instabilities was studied using an azimuthal array of high-frequency magnetic probes (figure 1*c*). Each probe consisted of a single square-shaped turn of copper wire with an area of 1 cm^2, insulated by Teflon, oriented azimuthally and spaced apart at steps of 7.5°. One of the probes had an additional radially oriented turn, so that the polarisation of the magnetic perturbation in the (r, φ) plane could be determined. The probes were capable of recording signals with frequencies of up to 100 MHz. The signals were recorded with an ADC at the rate of 500 MSamples s^{-1}.

The array was installed at the location with the local mirror ratio $R = 1.44$ perpendicularly to the GDT axis. Each coil's centre was located 21 cm away from the axis, as placing them any closer leads to perceptible fast ions losses. The radius of the magnetic surface touching the limiters and serving as the warm plasma boundary was 13.7 cm. Since the plasma in the GDT centre can have a β of up to $\approx$10 % (with an obtained maximum of approximately 60 % at a turning point demonstrated in Bagryansky *et al.* 2011), the probes were capable of measuring the properties of the plasma instabilities through the associated magnetic field perturbations despite the remoteness of the probes.

https://doi.org/10.1017/S0022377824001399 Published online by Cambridge University Press

Additionally, a longitudinal array consisting of similar magnetic probes was used in this study. Six probes measuring the axial component of magnetic field perturbations were distributed over the length of the region between the centre and the western fast ion turning point (figure 1*a*,*c*).

2.3. *Electrostatic probes*

An array of electrostatic probes was used to corroborate the magnetic probe data. The array (figure 1*d*) was installed right in front of the western limiter, at the local mirror ratio of $R = 4.33$. Placing it far away from the fast ion confinement region allowed us to move these probes close to the plasma edge without disrupting the plasma. Each of the eight probes consisted of a molybdenum wire of 0.2 mm diameter shielded by a copper tube grounded to the vacuum chamber. A thin silica glass tube insulated the wire from the shield, and another glass tube insulated the copper shield from contact with the plasma and the metal base of the array. A 5 mm long Mo-wire tip protruded beyond the shield and served as the antenna. The probe tips were located at 10° steps along the arc with an 8 cm radius, which is the radius of the plasma column at this location.

For another experiment where we measured the phase shift between the probe signals at different radii (figure 1*e*) four of those eight probes were arranged into two pairs. Because of the high heat flux that the probes would experience in the GDT, instabilities could not be investigated across the entire plasma cross-section and measurements had to be conducted at the plasma edge where the probes could withstand the heat. In each pair one probe touched the plasma edge (probes numbered 3 and 5, figure 1*e*) and the other was slightly removed from the edge radially (probes 8 and 7 at distances of 1 and 2 cm from their counterparts, respectively). They were also spaced from each other along the GDT axis by 12 mm, which was accounted for during evaluation of the perturbation's radial wavelength (with limitations specified in § 3.4).

There was only one ADC capable of recording electric and magnetic probe signals, so either magnetic or electrostatic probe signals were being recorded at a time.

2.4. *Data processing technique*

An electromagnetic perturbation δU can be represented as a superposition of azimuthal modes m due to the cylindrical geometry of a magnetic mirror trap

$$\delta U(t, r, \varphi, z) = \sum_m \delta U_m(t, r, z) \exp(\mathrm{i}m\varphi). \tag{2.1}$$

The analysis of a perturbation's azimuthal structure is based on the assumption that a single azimuthal mode of the instability dominates during its development.

Instabilities in discharges were observed as sequences of self-correlated independent oscillation bursts with their correlation times ranging from 5 to 100 μs (figure 5*a*,*b*). An instability's spatial structure can be constant during time periods under 100 μs, and a new instability with the same frequency but different spatial properties can form while the previous one decays. Hence, the decision was made to process probe data in short time windows of either 5 or 10 μs.

Every window underwent the following processing before being subjected to FFT. First, the offset and the linear slope were subtracted from the signal data. After that, the window was multiplied by the Hanning window and extended fourfold by appending zeroes to obtain better spectral resolution. Then, having obtained Fourier images $U_x(f)$, $U_y(f)$ of the simultaneous windows $u_x(t)$, $u_y(t)$ of probes x and y, the complex cross-spectrum was

https://doi.org/10.1017/S0022377824001399 Published online by Cambridge University Press

calculated as

$$C_{x,y}(f) = U_x^*(f)U_y(f) = P_{x,y}(f)\exp[\mathrm{i}\Theta_{x,y}(f)], \tag{2.2}$$

where the cross-power $P_{x,y}(f)$ denotes the frequency domain of the signals' congruence and the cross-phase $\Theta_{x,y}(f)$ is the phase difference between the two signals. This procedure was applied to signals from all pairs of adjacent probes (n in total), giving $n-1$ cross-powers and cross-phases.

The cross-power magnitude can be used to identify time–frequency regions with reliable signal correlation according to the criterion from Scargle (1982, expression 18). This criterion is applied in § 3.2 for analysis of electrostatic probe signals. These time–frequency regions were combined for $n-1$ pairs of adjacent probes and the cross-phases were averaged across the resulting region. For electrostatic probes such values of the azimuthal wavenumber m were chosen for which the standard error did not exceed $\Delta m = 0.5$; whether the procedure worked correctly was determined by visual inspection of the obtained data.

Magnetic probes collected much more data, therefore these data had to be processed automatically. The time–frequency regions had to be chosen differently: in each time interval a more narrow vicinity of the spectral maximum was chosen than the criterion allows. As the result, the data samples taken from the magnetic probe data were even more statistically reliable. The phase shift $\Theta_{x,y}$ between remote magnetic probes (i.e. probes that have other probes between them) x and y in the azimuthal array is given by $\Theta_{x,y} = \sum_{i=x}^{y-1}\Theta_{i,i+1}$, where $\Theta_{i,i+1}$ is the cross-phase of adjacent (to each other) probes i and $i+1$. If only one azimuthal mode is present, the dependence of these phase shifts on the angular distance between the probes x and y is linear, and m is given by the slope of the line. This way the wavenumber m can be determined for each 5 or 10 μs observation window of the instability evolving.

During the magnetic probe data processing, we used two criteria to determine whether a mode was present in a discharge. The first criterion was that the coefficient of determination of the fit line R^2 had to exceed 0.85. The second criterion was that all values of the phase shift between adjacent probes had to have the same sign (a single value, however, was allowed to differ). The described criteria were not applicable to the case of $m = 0$, since the phase shifts were small and had random signs.

Bicoherence squared b^2 was estimated to determine nonlinear coupling between the fluctuation components with frequencies f_1 and f_2 using

$$b^2(f_1, f_2) = \frac{|\langle U(f_1)U(f_2)U^*(f_1+f_2)\rangle|^2}{\langle|U(f_1)U(f_2)|^2\rangle\langle|U(f_1+f_2)|^2\rangle}, \tag{2.3}$$

where the angular brackets $\langle\ldots\rangle$ denote averaging over signal windows.

2.5. *Target plasma composition control*

The isotopic composition of the target plasma was adjusted by mixing D_2 and H_2 and using the mixture in both the initial gas target and in the arc discharge plasma gun. The mixture was prepared in corresponding reservoirs and its composition was controlled via pressure gauges.

An auxiliary series of experiments was conducted to determine if the composition of the target plasma corresponded exactly to the composition of the gas mixture used. A spectrometer and an optical system similar to the one described in Lizunov *et al.* (2011) as a part of the MSE diagnostic were used to measure the percentage of deuterium in the plasma during the discharge. The optical system (10 in figure 1*a*) collected radiation

https://doi.org/10.1017/S0022377824001399 Published online by Cambridge University Press

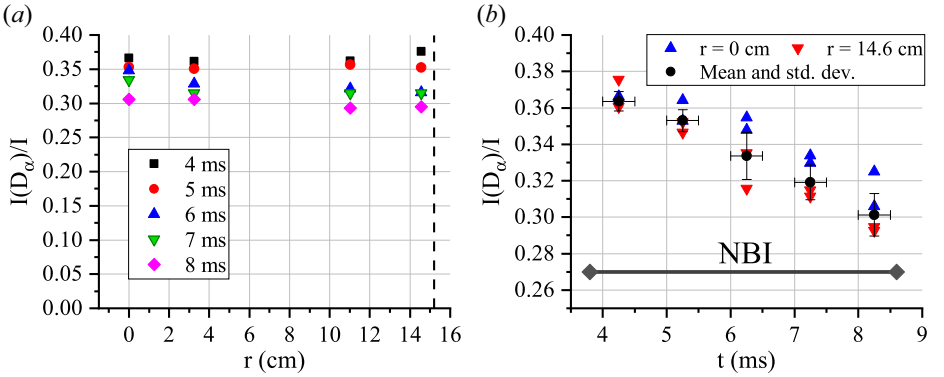

FIGURE 2. The D_α contribution to the total spectral density integral in the vicinity of spectral lines for both H_α and D_α in the 36 ± 3 % D_2 target plasma: (*a*) temporal dependence for different chord radius central plane projections; the dashed line shows the limiter edge projection onto the central plane; (*b*) temporal dependence of $I(D_\alpha)/I$ during NB injection for two particular radii (triangles) and the mean values over all the measured radii (circles).

along four chords in the plane perpendicular to the GDT axis and at different distances from the axis. The time of exposure start was varied while the exposition time of 0.5 ms remained constant. The registered radiation belonged to a spectrum range including H_α and D_α lines, which were well resolved by the spectrometer. The ratio between the D_α line intensity (spectral density integral in the vicinity of the spectral line, $I(D_\alpha)$) and the total intensity of both spectral lines I was taken to be the percentage of deuterium in the plasma. This follows from the assumption that the excitation rate coefficients for radiation emission at H_α and D_α frequencies are the same. This assumption is justified due to the same energy structure of deuterium and hydrogen (neglecting the isotopic shift) and the high speed of electrons far exceeding that of the ions; however, due to that high speed both warm and fast ions contributions are accounted for, both of which are considerable.

Figure 2(*a*) shows the D_α contribution to the total intensity depending on the chord-to-axis distance projected on the central plane. The results are plotted for several different exposure start times. The deuterium fraction in plasma was constant across the plasma column radius (with a relative error not exceeding 7 %) up to the limiter edge projection onto the central plane (black dashed line in figure 2*a*), but dropped during a discharge. It can be seen more clearly in figure 2(*b*) that the deuterium content decreased by approximately 18 % during the NBI. Such decline could be caused by hydrogen accumulating in the plasma because of its desorption from the first wall and the limiters as well as because of unnoticed leakage of the water vapour into the vacuum chamber. Bearing in mind that the used gas mixture contained 36 ± 3 % of deuterium, as determined from partial pressures, we concluded that at the start of the NB injection the deuterium fraction in the plasma was the same as in the prepared gas mixture, and that the deuterium content was uniform across the viewed cross-section.

3. Results and discussion

3.1. *Ion-cyclotron instabilities*

An instability with a frequency of approximately 2.2 MHz (figure 3*a*) was observed in pure hydrogen target plasmas as well as in plasmas with specific hydrogen–deuterium ratios (more on the ratios in § 3.3). The frequency of the instability was close to the ion-cyclotron (IC) frequency of deuterium in the GDT centre (2.74 MHz). Varying

https://doi.org/10.1017/S0022377824001399 Published online by Cambridge University Press

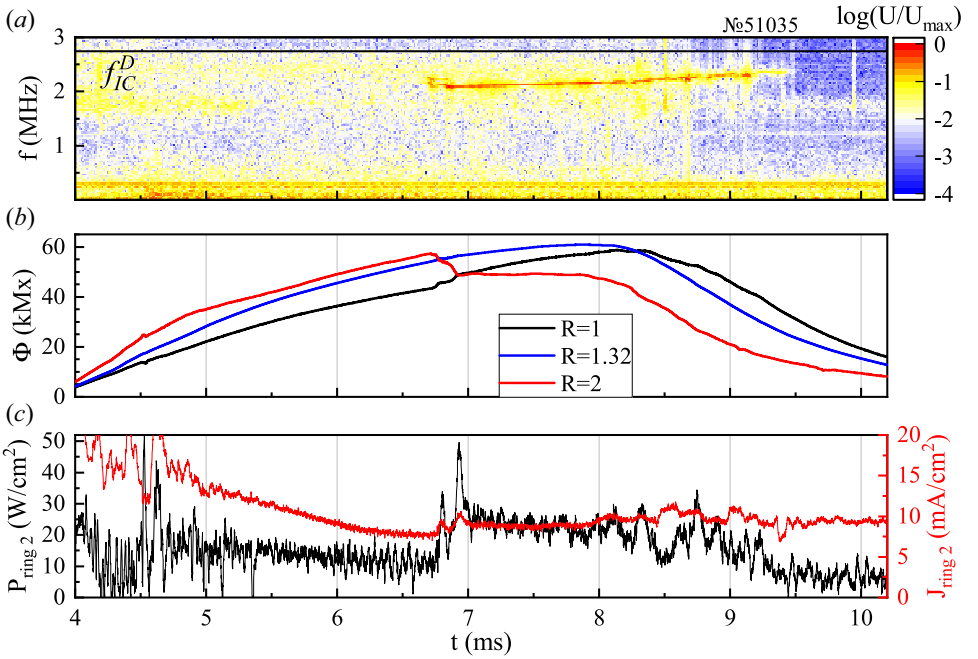

FIGURE 3. Data from a discharge with a 2.2 MHz instability (no. 51035): (*a*) spectrogram of a magnetic probe signal during an instability evolving in a discharge with a mixed hydrogen–deuterium target ($\langle n_e l\rangle = (2.9 \pm 0.4) \times 10^{14}$ cm^{-2}, 46 % deuterium mixture). The black line marks the IC frequency of deuterium in the GDT centre; (*b*) diamagnetic flux signals from the diamagnetic loops; (*c*) power and ion current fluxes from a bolometer and ion current probe pair on the plasma absorber.

the magnetic field strength proportionally changed the instability frequency, confirming its IC nature. The discrepancy Δf between the instability and IC frequencies could arise from the local magnetic field strength decreasing due to plasma diamagnetism, as suggested by Turner *et al.* (1977). However, in our case this is unlikely since during a discharge the instability frequency changes only slightly while the diamagnetic flux changes significantly (see figures 3*b*, 4*a*, 4*c*) and Δf exceeds the expected value of $\Delta f/f = 1 - \sqrt{1-\beta} < 0.05$ for the maximum value of $\beta \lesssim 0.1$ in the central plane. Moreover, the Doppler shift of the instability frequency due to the $\boldsymbol{E} \times \boldsymbol{B}$ plasma rotation ($\sim$10 kHz) can be neglected. The discrepancy could also be explained by the fact that non-local analysis of DCLC modes in a cylindrical geometry (Ferraro *et al.* 1987) predicts the DCLC to appear at a frequency significantly lower than that of the IC, but proper comparison would require taking into account longitudinal inhomogeneity, the radial distribution of fast ions (which differs from pure Gaussian) and finite beta and finite Larmor radius effects.

Figure 4(*a*) illustrates the instability at a frequency of approximately 4.5 MHz that formed in pure deuterium plasmas. As in the previous case, its frequency was proportional to the magnetic field strength, i.e. it also had an IC nature. This instability's frequency was close to both the second harmonic of the deuterium IC frequency in the GDT centre and the IC frequency associated with the magnetic field at the turning points ($R = 2$), which was equal to 5.48 MHz.

The 4.5 MHz instability seemed to originate as both an independent instability at the turning point and as a result of nonlinear coupling of the 2.2 MHz instability near the

https://doi.org/10.1017/S0022377824001399 Published online by Cambridge University Press

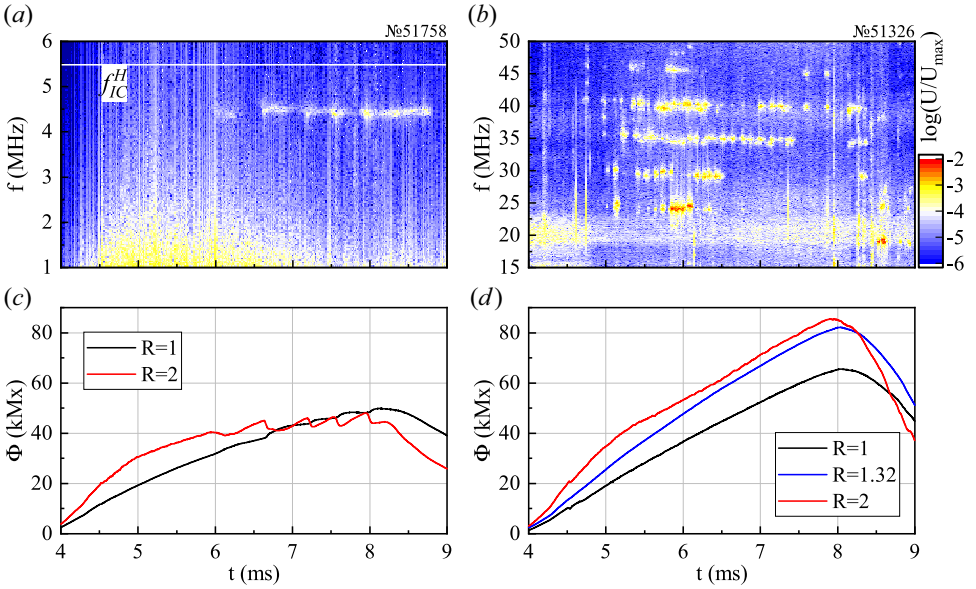

FIGURE 4. Instabilities evolving in the discharges with a pure deuterium target under (*a*) moderate plasma density $\langle n_e l\rangle = (2.9 \pm 0.3) \times 10^{14}$ cm^{-2} and (*b*) high plasma density $\langle n_e l\rangle = (4.9 \pm 0.3) \times 10^{14}$ cm^{-2}; (*c*,*d*) corresponding diamagnetic flux signals.

trap centre. Figure 5(*c*) shows the spectra of three probe (7 on figure 1*a*) signals that were obtained in a plasma discharge with a pure hydrogen target. If the two instabilities are flute-like in nature, the probes at different locations must be probing the same wave; thus, by the amplitude of the signal their point of origin can be traced. The highest spectral peak at 2.2 MHz belonged to the probe closest to the centre ($R = 1.19$), while the highest spectral peak at 4.5 MHz belonged to the probe near the turning point ($R = 2.1$). The signal from the probe located near the azimuthal array ($R = 1.47$) had the weakest spectrum peaks at both aforementioned frequencies. This can be interpreted as the 4.5 MHz instability principally arising in the vicinity of turning points independently from the 2.2 MHz instability. The instability evolving near the turning point has been observed in Berzins & Casper (1987), where its localisation was reliably determined by skewing the neutral beams. It has been demonstrated in Ferron & Wong (1984) that several DCLC modes with various frequencies can originate at different points where particle–wave resonance is effective, in particular, in regions with $\nabla B \approx 0$. On the other hand, b^2 (calculated from an azimuthal magnetic probe data at $R = 1.44$, figure 5*d*) peaks at $f_1 = f_2 \approx 2.2$ MHz, suggesting that it is the nonlinear coupling of the 2.2 MHz instability that is the reason of the additional 4.5 MHz spectrum component formation.

Whenever instabilities formed, simultaneous changes in diamagnetic flux signals were observed (figures 3*b* and 4*c*). The drops in the $R = 2$ loop signal coincided with rises in other loops signals, especially the central loop ($R = 1$). Additionally, simultaneous spikes in power and ion fluxes on the plasma absorber were recorded (figure 3*c*). This suggests that the instability caused scattering of fast ions (since they are the ones that primarily contribute to the diamagnetic flux signals) and redistributed the diamagnetic pressure along the trap axis, smoothing the maxima of the axial pressure profile.

The instabilities were observed in different discharges with the linear electron density $\langle n_e l\rangle$, measured with the dispersion interferometer (9 in figure 1*a*), ranging from 2.3×10^{14}

https://doi.org/10.1017/S0022377824001399 Published online by Cambridge University Press

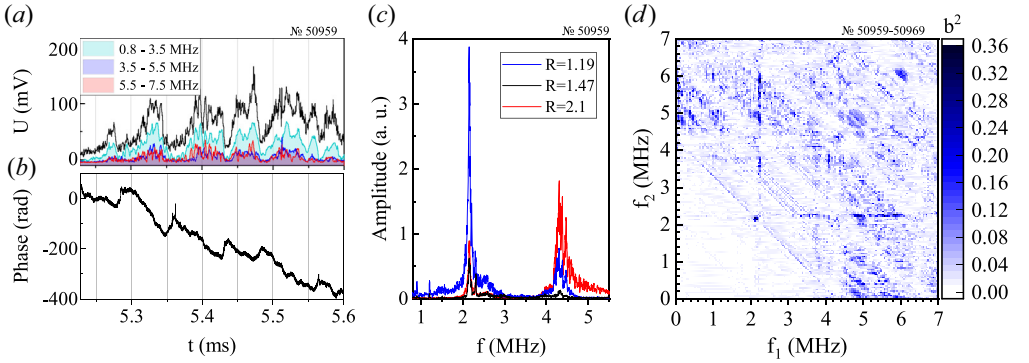

FIGURE 5. (*a*) Envelope of the raw magnetic probe signal ($R = 1.44$, black line) and envelopes of this signal passed through several band-passes that correspond to the base frequency and its second and third harmonics. (*b*) Time dependence of the phase in the range of 2–2.5 MHz which includes the base frequency; (*c*) signal spectra of three magnetic probes installed at different local mirror ratio points (7 in figure 1*a*); (*d*) bicoherence squared calculated from a probe signal ($R = 1.44$) by averaging 200 time windows with 23 μs duration each.

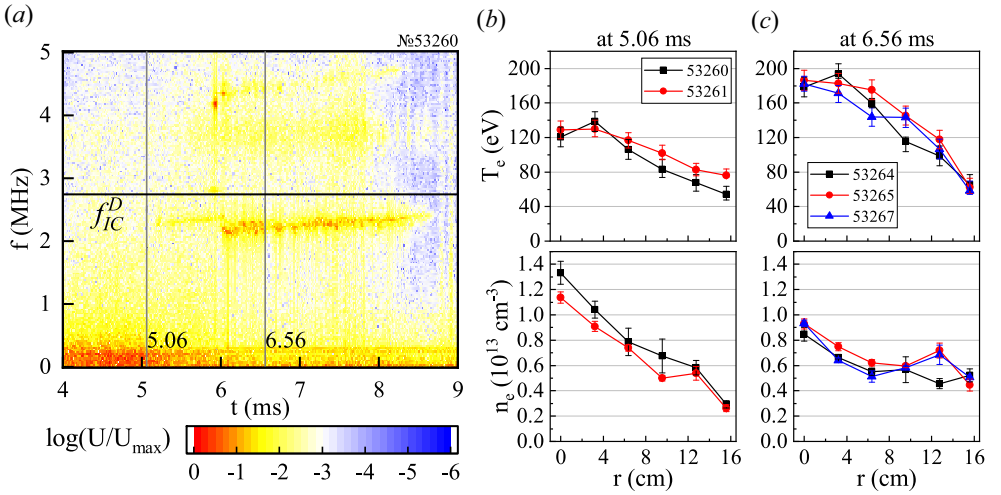

FIGURE 6. (*a*) Spectrogram of a 2.2 MHz instability registered with an electrostatic probe. Vertical grey lines denote time points at which radial profiles of (*b*) electron temperature and (*c*) density were measured.

to 3.6×10^{14} cm^{-2}. For a typical discharge with a hydrogen target characterised by a time-averaged (from 5 to 9 ms) value of $\langle n_e l \rangle = (2.9 \pm 0.2) \times 10^{14}$ cm^{-2} (from here on out, the provided $\langle n_e l \rangle$ values denoted the mean ± standard deviation on the time interval), figures 6(*b*) and 6(*c*) show radial profiles of electron temperature T_e and density n_e obtained with the Thomson scattering diagnostic before and during the instability. During the discharge T_e values increased due to NB heating, while the n_e profile, that initially peaked near the axis, flattened. Although we cannot infer how the instability affected the plasma parameters specifically and how the plasma density profile change influenced the instability, these data allowed us to determine the conditions in which it exists in the GDT.

https://doi.org/10.1017/S0022377824001399 Published online by Cambridge University Press

Increasing the linear plasma density to $\sim 5 \times 10^{14}$ cm^{-2} by operating the second gas valve allowed us to completely avoid the 4.5 MHz instability in pure deuterium plasmas and almost entirely suppress the 2.2 MHz instability in pure hydrogen plasmas. This observation is in line with what we expect from the DCLC instability, i.e. its being suppressed by increasing the warm ion density, thus filling the loss cone.

High-frequency instabilities were also observed in mixed deuterium–hydrogen plasmas of both moderate and high densities. A pure deuterium discharge is shown in figure 4(*b*), in which we observed a few harmonics ranging from approximately 25 to 80 MHz in steps of approximately 5 MHz, which was the deuterium IC frequency at the fast ion turning points. These harmonics were also observed in microwave radiation power spectra during the collective Thomson scattering (CTS) diagnostic implementation experiments on the GDT (Shalashov *et al.* 2022). Nonetheless, this instability did not influence the diamagnetic flux (figure 4*d*) noticeably and thus we did not investigate it further during this study.

An increase in the target plasma density, in combination with the proper tuning of the gas puffing duration, allowed us to raise the power captured by the plasma from the NBI (up to $\approx$2.5 MW) as well as the diamagnetic flux (over $\approx$70 kMx in the central plane) in a pure deuterium target discharge. Thus, with increased neutral gas puffing, β exceeded the stability threshold and the Alfvén ion-cyclotron instability (AICI) formed, which caused fast ions to scatter and limited the diamagnetic flux growth rate. Besides, increased density of the target plasma contributed to the AIC instability's arising because it decreases the Alfvén wavelength and thereby weakens the effect of the longitudinal magnetic field inhomogeneity on stabilisation (Watson 1980). At linear density values of 6.0–6.7 $\times$ 10^{14} cm^{-2} the 2.2 and 4.5 MHz instabilities were suppressed and only AIC instability developed (more in § 3.4). These values were obtained in pure deuterium targets; as this study was mostly focused on DCLC instability, the influence of target plasma composition on AICI was not investigated.

As shown previously in Zaytsev *et al.* (2013, 2014), the AIC instability in the GDT develops at the base frequency of 1.3 MHz or less and with the azimuthal wavenumber of $m = 1$. In our experiments, using electrostatic probes we observed the same AIC instability being self-correlated during its entire lifetime (approximately 1 ms) and disappearing after NBI ended. Determination of its azimuthal wavenumber, which turned out to be $m = 1$, allowed us to verify the signal processing procedure described previously in § 2.4. The following sections show that spatial properties of the 2.2 MHz instability were different from those of the AICI, therefore, the features of the observed AIC instability clearly show that the instabilities at 2.2 and 4.5 MHz have a different nature. Further on, we will refer to the 2.2 MHz and 4.5 MHz oscillations as the DCLC instability since their properties satisfy its description.

3.2. *Azimuthal structure of the DCLC instability*

For discharges with a pure hydrogen target and the strong 2.2 MHz instability, electrostatic probe signals were processed in steps of 10 μs with 30 μs windows. Within each window instabilities were distinguished in cross-power spectrum using the detection threshold from Scargle (1982, expression 18). Phase shifts in the common time–frequency domain among all pairs of the adjacent probes were averaged to plot colour maps displaying normalised azimuthal wavenumbers $m = k_\varphi r_{pl}$ within this domain (figure 7*a*,*b*).

It can be seen that the way the instability develops depended on the target plasma density: at low density $\langle n_e l \rangle = (2.2 \pm 0.2) \times 10^{14}$ cm^{-2} the instability started as high-amplitude (figure 7*c*) narrow-band oscillations with apparent positive azimuthal wavenumbers in the 1–5 range and continued as wider band low-amplitude oscillations

https://doi.org/10.1017/S0022377824001399 Published online by Cambridge University Press

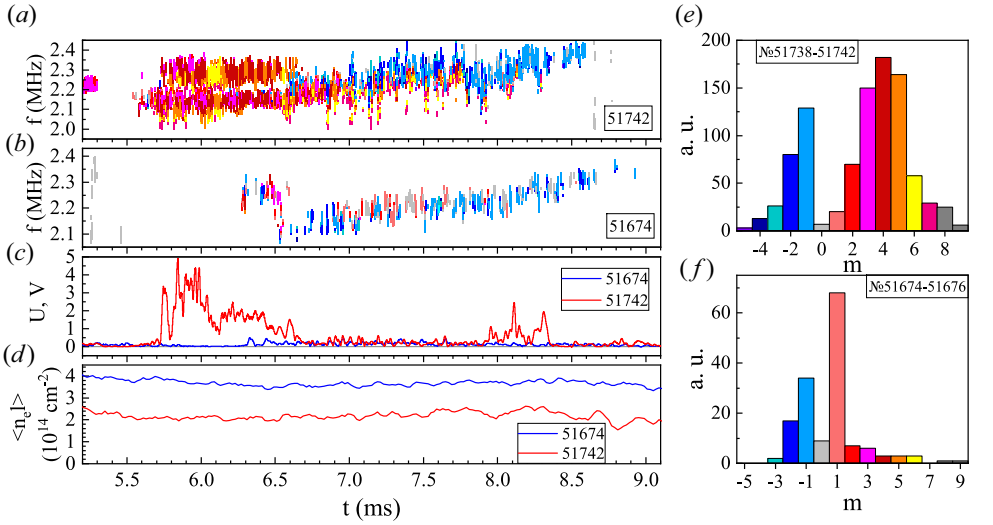

FIGURE 7. (*a*,*b*) Time dependencies of azimuthal wavenumbers (distinguished by colour) of the 2.2 MHz instability for two discharges with different plasma densities; (*c*) envelope curves of electrostatic probe signals band-pass filtered between 1.9 and 2.6 MHz (smoothed over 30 μs) and (*d*) time evolution of the linear electron density in these discharges; (*e*,*f*) distributions of azimuthal wavenumbers for two groups of discharges: (*e*) the low density $\langle n_e l\rangle = (2.2 \pm 0.2) \times 10^{14}\mathrm{cm}^{-2}$ case, (*f*) the higher density $\langle n_e l\rangle = (3.6 \pm 0.2) \times 10^{14}\ \mathrm{cm}^{-2}$ case.

with widely spread wavenumbers. At higher density $\langle n_e l\rangle = (3.6 \pm 0.2) \times 10^{14}\mathrm{cm}^{-2}$ the instability immediately started as low-amplitude, wide-band oscillations with absolute values of its wavenumbers close to unity. To support these observations, distributions over two groups of discharges, related to either lower density or higher density, are shown in figures 7(*e*) and 7(*f*), respectively. Note that the change in how the instability develops in the low density case is not connected to variations in $\langle n_e l\rangle$ during a discharge (figure 7*d*). This change could be caused by modification of the radial warm ion density profile during a discharge that was expected for the DCLC instability and has been observed in Koepke *et al.* (1986) and Ferron & Wong (1984).

When the instability began to develop and had a high amplitude at low plasma densities, its wavenumbers were positive, which means that it propagated in the ion diamagnetic drift direction. This feature is compatible with properties of the DCLC instability. However, when the instability evolved at a lower amplitude (especially at high plasma densities), its wavenumbers became partly negative and smaller in absolute values. These features mean a larger scale of the instability spatial structure and propagation in the electron drift direction. The latter is not typical for the DCLC instability, although it has been observed earlier by Turner (1977).

Swift changes in azimuthal wavenumbers (especially between 5.6 and 6.6 ms in figure 7*a*) agree with our understanding that that the instability evolves as a sequence of separate short oscillations (also seen in figure 5*a*,*b*). This might be explained by a build-up of a drift wave by a group of fast ions leading to scattering of the said ions and thus the resonance conditions' breaking. As the result, the instability decayed, but a new one formed in its place due to the NBI supplying new fast ions. However, the instability did not necessarily scatter the resonant ions. Another mechanism of an instability's intermittence (bursting) was proposed in Ferron & Wong (1984). The authors

https://doi.org/10.1017/S0022377824001399 Published online by Cambridge University Press

observed the DCLC instability, whose frequency, wavelength, phase velocity and the radial profile of the amplitude all satisfied the resonance conditions and the requirement for the azimuthal wavenumbers to be integer. Since plasma parameters changed, it could be that a dominant saturated mode with a given wavenumber no longer satisfied the requirements, and another one, that did satisfy them, grew to became dominant. The amplitude bursting took place simultaneously at different azimuthally and radially located points, so the plasma was unstable in its entire cross-section. On the contrary, on the same LAMEX machine (Leikind *et al.* 1985) it was shown that, besides the aforementioned reasons, the instability bursting can be caused by its spatial localisation, with bursts arising when a spatially localised mode passes by the probes as a part of a large-scale convective plasma motion.

In our case, all of these effects could be responsible for the instability bursting. However, it is the scattering of the resonant ions and hence the resonance breaking that is most likely to be the main reason of the bursting, due to high estimated energy of the lost ions (§ 3.5). It is difficult to determine if the other effects were responsible for bursting because of the small size of both probe arrays (45° and 70°) and because of the ongoing NB injection, whereas in the reported experiments (Ferron & Wong 1984; Leikind *et al.* 1985) the instability developed during free decay of plasma.

3.3. *The DCLC in plasmas of different compositions*

Ion-cyclotron instabilities at frequencies between 2.2 and 5 MHz were observed in discharges with pure hydrogen and deuterium target plasmas as well as in experiments with varying isotopic target plasma compositions. The experimental series with magnetic probe measurements was characterised by $\langle n_e l\rangle$ between 2.3×10^{14} and 3.6×10^{14} cm^{-2} (with a mean value of $\langle n_e l\rangle = (3 \pm 0.4) \times 10^{14}$ cm^{-2}). The edge values of this range correspond to the two target plasma densities used in wavenumber measurements with electrostatic probes. Thus, it would be reasonable to expect similar values of the azimuthal wavenumbers measured by magnetic probes, and indeed, they were mainly distributed between 2 and 6 for both measurements taken by magnetic probes and by electrostatic probes in low density plasmas (figures 8*b* and 7*a*). However, negative wavenumbers were almost invisible to the magnetic probes, which could be due to the stricter selection criterion used in their data processing compared with electrostatic probes (see § 2.4).

The 2.2 MHz instability formed in every discharge until the deuterium content in the target plasma exceeded 54 %. This instability had a narrow enough spectrum to process the probe signals using the technique described in § 2.4. These signals were processed in windows of 5 μs to obtain temporal dependencies of the azimuthal wavenumber as well as the perturbations polarisation $\theta_{r-\varphi}$ in the plane almost normal to the magnetic field. The latter is the phase difference between signals from r- and φ-oriented coils of the magnetic probe. The results are shown in figure 8(*a–c*). The frequency distributions in figure 8*a* have a wide spread. The reason for this is that these distributions were made using the data from the entire duration of the discharges, thus they were affected by the instability frequency's drifting during the discharge.

The normalised azimuthal wavenumber m ranged from 1 to 7 for all target plasma compositions with values in the 2–5 range dominating in most cases (figure 8*b*) with no specific time dependence. Thus, we cannot conclude that the azimuthal structure of the instability depended on deuterium content. The unstable waves propagated in the ion diamagnetic drift direction regardless of the target composition.

The polarisation angle distribution was almost uniform and its values were mostly positive in pure hydrogen target plasmas (figure 8*c*). However, as deuterium content increased, a well-defined maximum became sharper and gravitated to $\pi/2$. Since

https://doi.org/10.1017/S0022377824001399 Published online by Cambridge University Press

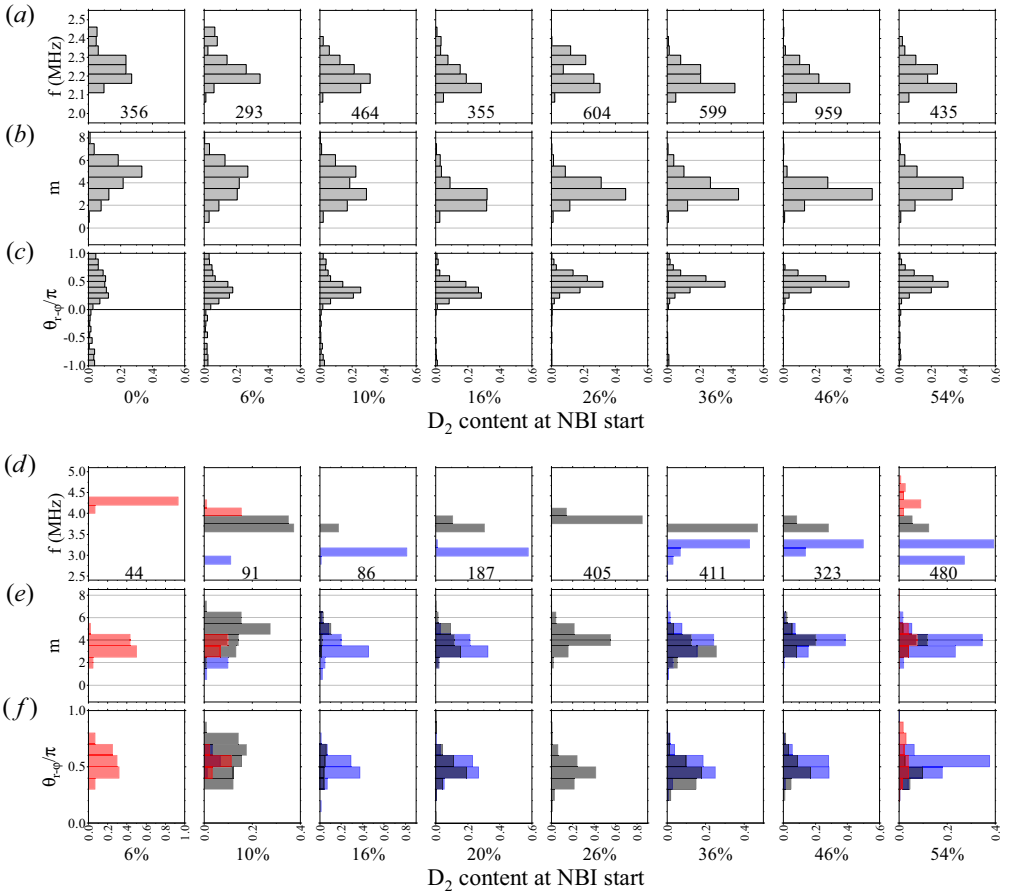

FIGURE 8. Properties of the instability at: (*a–c*) the base frequency of approximately 2.2 MHz, (*d–f*) the frequencies that are non-multiples of the base frequency: 4.2 MHz (red), 3.8 MHz (black) and 3 MHz (blue) versus deuterium content in the plasma target. For both cases: (*a, d*) the frequency distributions; (*b, e*) the normalised azimuthal wavenumber m distributions; (*c, f*) the distributions of the magnetic perturbation polarisation's $\theta_{r-\varphi}$ normalised by π. All histograms are normalised by total numbers of measurements (in (*a*) and (d) plots).

amplitudes of the r- and φ-oriented coils signals near 2.2 MHz are comparable, this means that the registered perturbations had a near-circular polarisation in the radial plane. This, however, is likely not a feature of the instability itself, but could be an effect caused by the probe remoteness from the core plasma, as magnetic perturbations in cold magnetised plasmas must be polarised circularly. The plasma column radius (taken to be the radius of the magnetic surface that touches the inner edge of the radial limiters) was approximately 14 cm in the plane where the probes were located, whereas the probes were located 21 cm away from the axis and immersed in the cold peripheral plasma.

In pure hydrogen target plasmas only the 2.2 MHz instability and its harmonics were observed; however, even with a small added amount of deuterium, instabilities at other frequencies, non-multiples of the base frequency, began to develop. Figure 8(*d–f*) demonstrates the properties of such instabilities grouped by their frequencies. Most instability azimuthal wavenumber distributions peaked at $m = 3$ or $m = 4$. Such instabilities arose mainly before the 2.2 MHz instability and lasted less time (see

https://doi.org/10.1017/S0022377824001399 Published online by Cambridge University Press

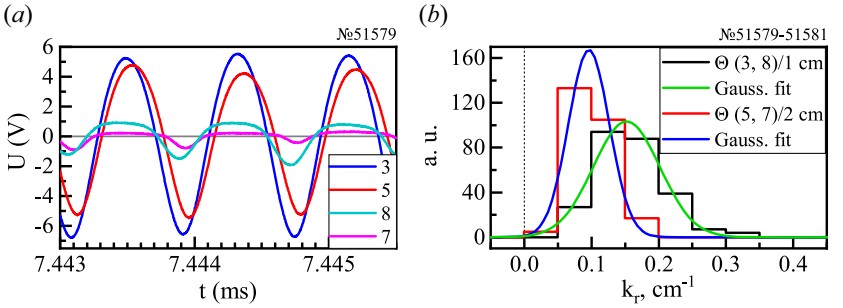

FIGURE 9. (*a*) The AIC instability registered with electrostatic probes (numbered according to figure 1*e*); (*b*) phase differences normalised by radial spacings between the probes.

figure 6(*a*) at 6 ms for instance). Azimuthal wavenumbers did not vary significantly while the instabilities developed. The instabilities propagated in the ion diamagnetic drift direction and the magnetic perturbations polarisation distributions had their maxima even closer to $\pi/2$ than in the 2.2 MHz case.

The deuterium content threshold under which the 2.2 MHz instability developed was between 54 % and 65 %. Of all DCLC-like instabilities, only the 4.5 MHz frequency and its harmonics remained when the deuterium content exceeded 65 %. Unfortunately, we were unable to determine the azimuthal wavenumbers of the 4.5 MHz instability since the phase shifts between the magnetic probes differed from each other significantly in their values and even in their signs. This could be due to different spatial modes' superposing as well as due to superposition of modes from both turning points.

3.4. *Radial structure of the AIC and DCLC instabilities*

Using pairs of radially displaced electrostatic probes (§ 2.3, figure 1*e*), we measured the radial phase shifts of DCLC and AIC instabilities on the plasma periphery.

The AIC instability amplitude decreased significantly with the distance from the plasma column (figure 9*a*), however, phase differences between the signals of the third and eighth probes, as well as between the fifth and seventh probes, were discernible. Different axial positions of radially distributed probes could contribute to the phase shift despite the AICI longitudinal wavelength $\lambda_\parallel = 136 \pm 4$ cm (Chen *et al.* 2022) far exceeding the distance between the paired probes along the axis (12 mm). The phase difference due to axial distance was $\Theta_\parallel = 0.06$ rad; it was subtracted from the measured differences between the probe signals. The radial wavenumber k_r could be obtained as the average of $(\Theta_{3,8} - \Theta_\parallel)/1$ cm^{-1} and $(\Theta_{5,7} - \Theta_\parallel)/2$ cm^{-1}, however, we chose a different method instead to highlight the discrepancy between phase differences for two probe pairs. We plotted the distributions of these phase differences normalised by the distances between the probes in pairs (figure 9*b*). The distributions show that we cannot consider the radial structure of the instability to be a single harmonic, i.e. $\sim \exp(ik_r r)$, so k_r should be understood as an inverted scale of perturbations. Both distributions were fitted with Gaussian curves to obtain the mean and the variance, and these values were used to calculate k_r as the weighted mean: $k_r = 0.11 \pm 0.03$ cm^{-1}. The corresponding AICI radial scale is $\lambda_r = 57 \pm 16$ cm, which significantly exceeds the plasma column radius. Presuming that the same value of λ_r is true for inside the core plasma as well, we can conclude that the AIC instability was uniform within the entire plasma cross-section, as proposed in Tsang & Smith (1987).

https://doi.org/10.1017/S0022377824001399 Published online by Cambridge University Press

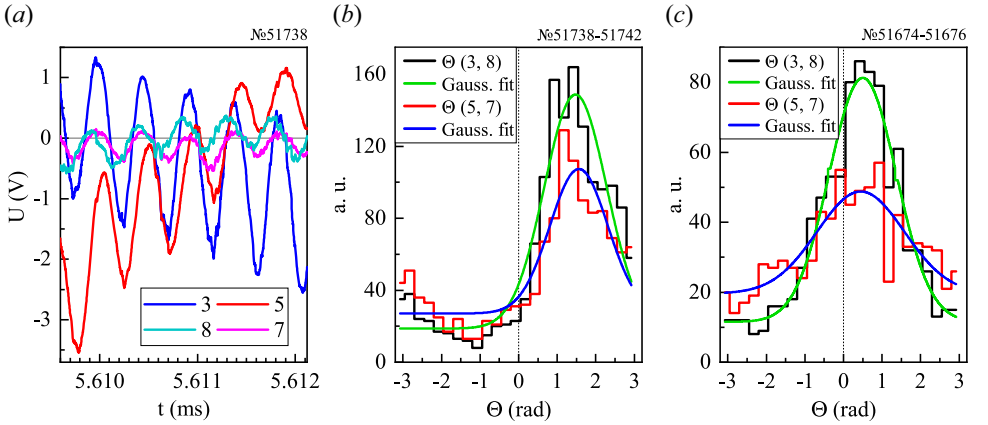

FIGURE 10. (*a*) The 2.2 MHz instability registered with electrostatic probes; phase differences for (*b*) the low plasma density $\langle n_e l\rangle = (2.2 \pm 0.2) \times 10^{14}$ cm^{-2} and (*c*) the higher plasma density $\langle n_e l\rangle = (3.6 \pm 0.2) \times 10^{14}$ cm^{-2} cases.

Figure 10(*a*) shows the amplitude drop of the 2.2 MHz instability with distance from the plasma edge. Assuming this to be the DCLC instability, we can consider its $k_\parallel \ll k_\perp$, neglecting the phase shifts between the probes in pairs 5–7 and 3–8 (figure 1*e*) due to their different axial positions. Figures 10(*b*) and 10(*c*) present distributions of phase differences between radially spaced probes in the same discharges as in figures 7(*e*), 7(*f*). Figure 10(*b*) shows results from several discharges with low linear electron density of $(2.2 \pm 0.2) \times 10^{14}$ cm^{-2}. Despite double the difference in distances between the probes, both distributions have almost the same mean values of 1.47 and 1.56 rad. Using these values and their corresponding variances, $k_r = 0.90 \pm 0.34$ cm^{-1} and the corresponding radial scale of the DCLC instability at low densities $\lambda_r = 7.0 \pm 2.6$ cm were derived. This value is approximately equal to the plasma column radius at the axial position of the probes. Similar distributions obtained for discharges with higher linear density $(3.6 \pm 0.2) \times 10^{14}$ cm^{-2} (figure 10*c*) had closer-to-zero mean values, so the corresponding k_r had to be smaller. The same was valid for m (figure 7*f*); thus we can conclude that the transverse scale of the instability tended to grow as the plasma density increased.

3.5. *Scattered ion energy estimation*

Using the plasma absorber diagnostics, we attempted to estimate the energy of lost ions. First, we examined the distribution of power and ion current over the area of the absorber. Plotting the fluxes averaged over each probe wing (45°, 135°, 225° and 315°) showed that the fluxes were independent of a probe's azimuthal angle (figure 11*a*), as expected due to the axial symmetry of the GDT. There was, however, a noticeable difference in power fluxes at different plasma absorber radii (figure 11*b*). When the fluxes were averaged over each ring of probes (i.e. over the same radius of the absorber), the highest peaks were observed at the radius of 28.2 cm, which, projected along the magnetic field lines in the GDT, corresponds to the radius of 7.3 cm in the central plane. The second highest peaks were observed at the absorber radius of 16.6 cm (4.3 cm in the central plane respectively); as for outer radii, no such sharp rises were observed. The ion current signals at these radii showed a similar behaviour, with the peaks at $r_2 = 28.2$ cm being the most prominent.

A numerical simulation of collisionless ion dynamics was carried out to obtain the spatial resolution of the bolometers. In this simulation, the ions were placed inside the

https://doi.org/10.1017/S0022377824001399 Published online by Cambridge University Press

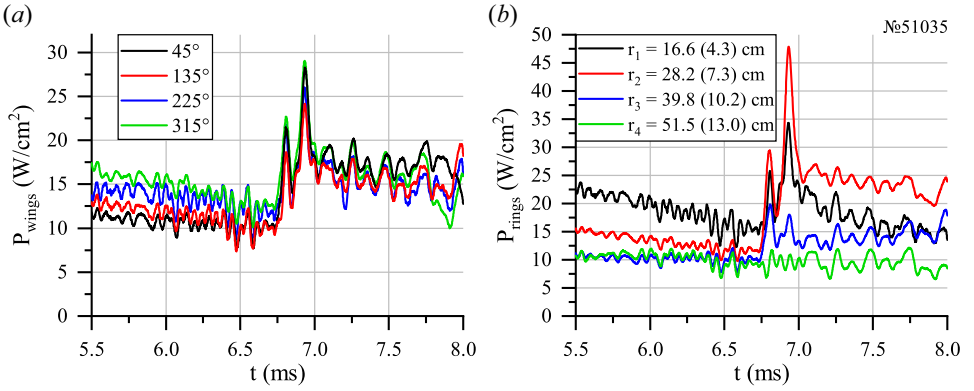

FIGURE 11. Examples of (*a*) azimuthal and (*b*) radial power flux distributions in a plasma discharge.

bolometer and allowed to fly apart isotropically, backtracking to their possible origins at the centre of the trap. Velocities and flight times of ions that reached the central plane were investigated as well as the radii at which they entered the central plane. The simulation showed that the spatial resolution did not exceed 3.3 cm in the radial direction for ions with 10 keV energies and the direct flight time τ_{flight} from the bolometers to the central plane was found to be approximately 6 μs.

Presuming the flux increases to be caused by instabilities, we attempted to verify if those losses could be the fast ions scattered from the centre of the trap. Assuming that the peaks of the bolometer signals were caused by scattered fast ion losses alone, we attempted to estimate their energy from the available data. To isolate these losses from the normal operational losses (henceforth referred to as 'background' losses), for both the power and ion current flux signals we fit straight lines into the short time period τ_{approx} before the instability formed (figure 12*a*). These straight lines, meant to simulate the background losses in the absence of the instabilities, were then extrapolated into the regions with the instabilities and deducted from the corresponding signals, bringing the power and ion flux signals to the same baseline. After that, we synchronised the flux signals to a magnetic probe signal with a 1.6–2.4 MHz band-pass filter applied programmatically. The band-passing was performed with the aim of tracking the appearance and growth of the 2.2 MHz instability. Having noticed that the magnetic probe, power and current signals had a similar shape shifted in time, we estimated the time delay τ_{delay} between the instability start and the ions reaching the absorber as the distance between the maxima of the signals (figure 12*b*). However, τ_{delay} is partially produced by the bolometer's response time of 15 μs. Additionally, we estimated the instability pulse length time τ_{inst}, which was used in the next step of the analysis.

By dividing the resultant backgroundless power flux by the backgroundless ion current (figure 12*b*), we obtained the time dependency of the energy per ion estimate E_{ion} (figure 12*c*). If the bolometer response time was taken into account, even higher estimates of E_{ion} would be obtained. Note that the values of the resultant dependency lie below the injected neutral beam's energy $E_{\text{inj}} = 24$ keV and above the background value of $E_{\text{back}} = 1.6 \pm 0.2$ keV, obtained by averaging the quotient of power by ion current (before subtracting the fit lines) over τ_{approx}. The resultant signal was then averaged over τ_{inst}, shifted forward from the instability start time by τ_{delay}. As the result, we obtained an estimate for the average energy per instability-scattered ion in the discharge. The procedure

https://doi.org/10.1017/S0022377824001399 Published online by Cambridge University Press

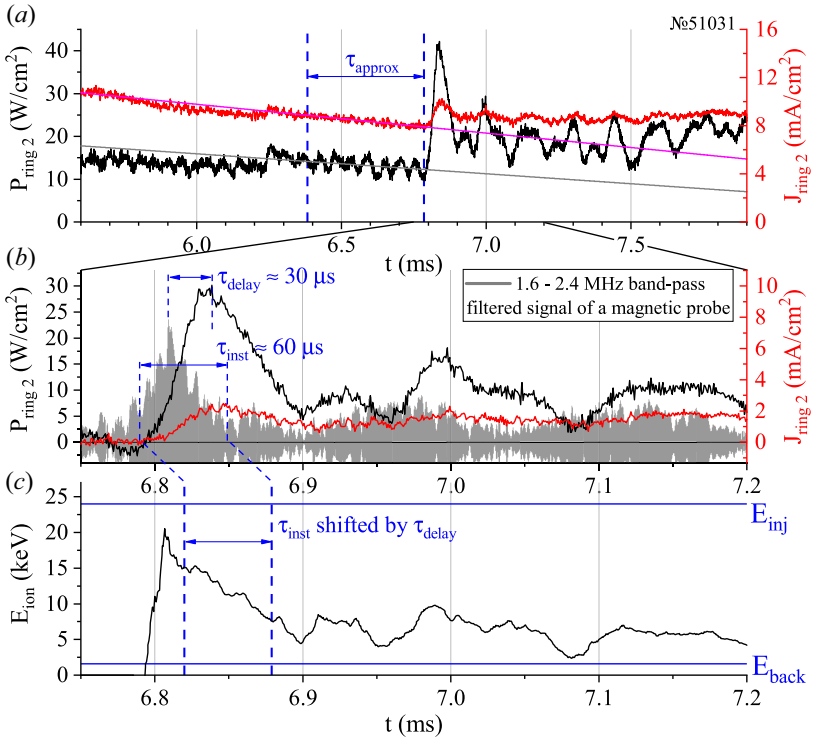

FIGURE 12. Visual guideline for the procedure used to determine the average energy of lost fast ions: (*a*) time period τ_{approx} before the instability was fit with a straight line to separate the instability-driven losses from background losses; (*b*) data were re-plotted with the fit lines subtracted, the magnetic probe signal was overlaid, τ_{inst} and τ_{delay} were determined; (*c*) graph of P_{ring2}/J_{ring2} was plotted and used to estimate the average energy of the ions lost due to the instability; additional blue lines correspond to the energy of injected neutral beams E_{inj} and the average energy of the background losses E_{back} calculated over τ_{approx}.

was repeated for 19 plasma discharges to obtain a range of average energy values. Some discharges, however, had several subsequent instability pulses in them. In these cases, we only analysed the first one, as we were unsure how the first pulse would affect the background flow for the following pulses.

In all the processed discharges, the estimated energy of instability-scattered ions ranged from 4 to 16 keV, with a mean and the standard deviation of 10 ± 4 keV. These values significantly exceeded the energies of the background losses, comprised mostly of warm ions E_{back}. In addition, we determined that the average τ_{delay} equalled 41 ± 3 μs.

We used the obtained results to estimate the transverse energy of the ions appropriate to fulfil the DCLC characteristic condition $k_\perp \rho_i \geqslant 1$. The majority of lost ions reached the plasma absorber from the central plane radius of $r_2 = 7.3 \pm 1.5$ cm with energies in the range of $E_{ion} = 10 \pm 4$ keV. One can expect that the DCLC instability has the highest amplitude at this radius. Using the measured value of $m = 4 \pm 2$ we obtained $k_\varphi = m/r_2 = 0.56 \pm 0.30$ cm^{-1}. Thereby, the condition $k_\varphi \rho_i \geqslant 1$ for the most unstable DCLC branches was satisfied for deuterons with transverse energies exceeding the threshold value ranging from 0.4 to 4.6 keV (depending on the value of k_φ). Taking k_r into account (projected to the central plane) gave a value for $k_\perp = 0.72 \pm 0.26$ cm^{-1} and somewhat different estimations of transverse ion energy: 0.3–1.5 keV.

https://doi.org/10.1017/S0022377824001399 Published online by Cambridge University Press

We also attempted to determine the region of the velocity space from which the ions were lost. Assuming that the instability (characterised by $f = 2.2$ MHz and $m = 4 \pm 2$) resonated with these ions, we evaluated their transverse velocities using

$$v_\perp = v_{\text{phase}} = \frac{\omega}{k_\perp} = \frac{2\pi f r_2}{m}, \tag{3.1}$$

and then obtained the pitch angle θ_{ion} using $\sin^2\theta_{\text{ion}} = m_D v_\perp^2 / 2E_{\text{ion}}$. The pitch angles of ions leaving the confinement region determined using this method turned out to be in the range of $\theta_{\text{ion}} = 14.7 \pm 8.6^\circ$, which is in line with the loss cone angle of $\theta_{lc} = \arcsin(1/\sqrt{R_{\max}}) = 9.9^\circ$. The value of θ_{ion} could be even closer to the loss cone angle if contribution of k_r to $k_\perp$ was used in the evaluation of $v_\perp$. Moreover, the average τ_{delay} between the moments when the DCLC bursts with the highest amplitude and when the power losses spikes for the first time equalled $\approx$40 μs. According to simulations, a 10 keV deuteron reaches the absorber in $\tau_{\text{flight}} \sim 6$ μs. In addition, our pyroelectric bolometer response time is 5 μs to register 50 % of an instant power flux pulse and 15 μs to register 90 %. Given the period of a single bounce oscillation $\sim$10 μs, the ions had to oscillate at least 2 or 3 times before reaching the plasma absorber. It follows that the lost ions had to already be near the loss cone in the phase space to get scattered by the instability in the collisionless regime. Therefore, it is possible that the DCLC-like IC instability developed by interacting with the ions located near the loss cone in the velocity space and eventually scattered them after a short time.

However, this method did not allow us to estimate energies of scattered ions when applied to the AIC instability. In regimes with the AIC instability the target plasma density and its longitudinal particle losses were several times higher than the corresponding density and losses in regimes with the DCLC instability, so the current of lost fast ions could not be discerned well from the background current. Additionally, there was an uncertainty in determining τ_{delay}. Direct measurements of the lost ions energy spectrum when AICI evolves were conducted in Anikeev *et al.* (2015*b*).

3.6. *Total losses caused by instabilities*

Energy and particle fluxes measured by probes on the diagnostic plasma absorber were integrated over its area under the assumption of uniformity of the fluxes within the sectors surrounding each probe. As the result, the total power P_{abs} and the total ion current J_{abs} of plasma leaving the trap through the western mirror were obtained. As seen in figure 13, both the 2.2 MHz DCLC instability (*a*) and the AIC instability (*b*) provoked an almost twofold temporary increase of total power losses and a relatively weak but discernible increase of the total ion current at the moment they arise. After the initial spike, the longitudinal energy losses, assumed to be caused by the DCLC instability, became almost constant but higher by $\approx$25 % than they were before the instability onset. In contrast, longitudinal power losses, caused by the AIC instability, increased for approximately 0.4 ms and later returned to the levels that would seemingly be observed in the absence of the instability. This can be interpreted as fast ions with pitch angle close to the loss cone angle being lost. These losses are driven by velocity diffusion of ions arising due to overlapping of $\omega - \Omega_i = n\Omega_b$ resonances, where Ω_b is the bounce frequency and n is some integer value (Chernoshtanov 2016, 2018). Such diffusion can scatter ions away from the vicinity of the loss cone in relatively short times (approximately tens of bounce periods), which are small in comparison with the relaxation time of the fast ion distribution due to Coulomb collisions. In addition, the AIC instability stays coherent over time intervals exceeding 1 ms. These observations correspond to the model in which AICI

https://doi.org/10.1017/S0022377824001399 Published online by Cambridge University Press

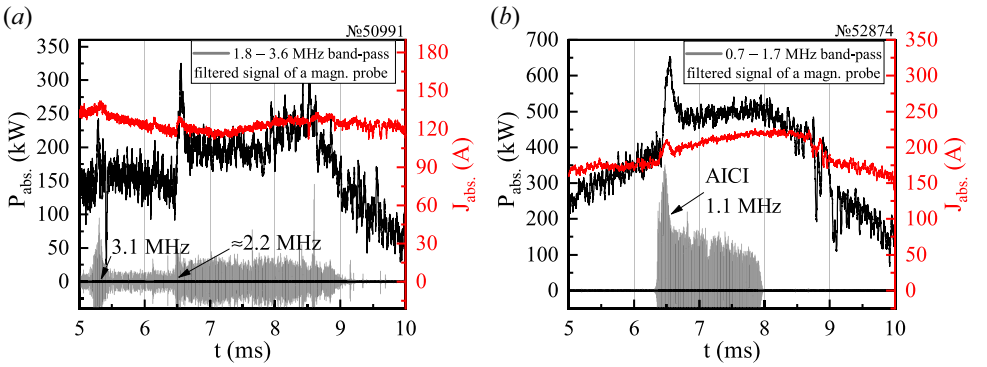

FIGURE 13. Total power (black) and ion current (red) measured by the absorber diagnostics synchronised with magnetic probe signals (rescaled for visibility): (*a*) DCLC-type instability; (*b*) AIC instability.

is excited by one group of ions and leads to anomalous losses of another group of ions (Chernoshtanov 2016, 2018) in contrast with the DCLC instability, which is excited by ions near the loss cone and scatters those same ions; after the ions are lost, the DCLC burst decays. However, we cannot be sure that additional energy losses due to AICI stop completely after a short period because the time dependence of losses under the same conditions but without the instability is unknown, as these conditions inevitably lead to the instability forming; the same is true for the case of the DCLC instability.

4. Conclusion

We conducted an experimental study of kinetic plasma instabilities in the GDT, a magnetic mirror device, with target plasmas composed of various mixtures of hydrogen and deuterium (as well as pure hydrogen and deuterium plasmas) with deuterium beam injection. In these experiments a number of IC instabilities were observed; of most interest to us were the instabilities with frequencies of 2.2 MHz and 4.5 MHz, which we determined to be drift cyclotron loss cone instabilities. Although other high-frequency (25–80 MHz) and AIC instabilities were also present, they were not investigated in depth because the former seemed non-crucial for fast ion confinement and the latter had been investigated in detail in previous studies.

The instabilities at frequencies of 2.2 MHz and 4.5 MHz were observed in plasma targets with the linear electron density in the GDT centre ranging from 2.2×10^{14} to 3.6×10^{14} cm^{-2}. These frequencies were close to the deuterium IC frequency in the GDT centre and in the fast ions turning points, respectively. The instabilities led to fast ion scattering, which was observed as drops in diamagnetic flux signals near turning points and increases in longitudinal energy and particle losses. With the use of plasma absorber diagnostics energies of the lost ions were estimated to be ranging from 4 to 16 keV.

Starting with a pure hydrogen target plasma, we gradually replaced hydrogen in the target mixture by deuterium. The properties of the 2.2 MHz instability did not change (the same properties of the 4.5 MHz instability could not be determined); however, when the deuterium content in the target reached a value between 54 % and 65 % the instability was suppressed entirely. As the deuterium percentage exceeded 65 %, the instabilities were only observed at 4.5 MHz, which presumably originated in the turning points as it could not be the result of nonlinear coupling of the absent 2.2 MHz instability. Increasing the plasma density to approximately 5×10^{14} cm^{-2} resulted in complete suppression of the

https://doi.org/10.1017/S0022377824001399 Published online by Cambridge University Press

instability in deuterium targets and reduced the instability impact on diamagnetic fluxes in hydrogen targets.

We attributed the 2.2 MHz instability to be a DCLC type because of its several features:

(i) the instability frequencies were multiples of the IC frequency;
(ii) addition of warm ions led to the instability being suppressed, which was most effective when the warm ions were of the same isotope as the fast ones;
(iii) the instability was small scale, i.e. its normalised azimuthal wavenumbers mostly ranged from 2 to 5;
(iv) the unstable wave propagated in the ion diamagnetic drift direction.

Despite this, we currently cannot experimentally confirm its flute-like nature. An aggregate of the data obtained for the 2.2 MHz instability allowed us to establish that it scattered ions located near the loss cone in the velocity space. This is in agreement with the fact that the instability developed in incoherent bursts and the estimation that the scattered ions performed a few bounce oscillations before being lost. Although the instability at 4.5 MHz behaved in the same way as the one at 2.2 MHz in relation to warm ion addition and the fast ion scattering, an uncertainty regarding its azimuthal structure did not allow to definitively identify it as a DCLC instability.

In view of this, we propose the following interpretation of the obtained results. A certain quantity of warm ions is needed to prevent the DCLC instability and the suppression is the most effective when the frequencies of the IC harmonics for warm and fast ions coincide. With oblique injection of the neutral beams the fast ion density profile has two maxima near the turning points, so a potential well for the warm ions forms between them (if $n_{\mathrm{fast}} \gtrsim n_{\mathrm{warm}}$). Thereby, the conditions required for the DCLC instability suppression occur in the trap centre vicinity first and foremost. Hydrogen plasma targets cannot suppress the instability at the first deuterium IC harmonic in the GDT centre, so the instability at 2.2 MHz is observed. The same situation remains in the case of mixed targets until the deuterium percentage of the target plasma exceeded 65 %. At the same time the amount of warm deuterium turns out to be insufficient for stabilising DCLC in the turning points regions, so the 4.5 MHz instability can appear even in plasmas composed entirely of deuterium and can only be suppressed by increasing the target density accordingly.

The evolution of the DCLC instability is a complex process, since it depends on several interrelated factors such as the degree to which the loss cone is filled with warm plasma, the isotopic composition of the plasma, the radial distributions of warm and fast ion densities as well as the axial distribution of the fast ion density. Therefore, the offered interpretation requires validation by numerical modelling of the fast ion distribution function while accounting for experimental conditions. Nonetheless, our results show that DCLC instability can be suppressed in the GDT by using two-species target plasmas, which improves the prospects of a GDT-based fusion neutron source.

Acknowledgements

Editor Cary Forest thanks the referees for their advice in evaluating this article.

Funding

The GDT maintenance, experiment conduction and data acquisition were supported by the Ministry of Science and Higher Education of the Russian Federation. Sections of the study concerning the probe data processing, determining DCLC instability properties and

DCLC suppression conditions analysis were supported by Russian Science Foundation (Grant No. 19-72-20139).

Declaration of interests

The authors report no conflict of interest.

REFERENCES

ANIKEEV, A.V., BAGRYANSKY, P.A., BEKLEMISHEV, A.D., IVANOV, A.A., KOLESNIKOV, E.YU., KORZHAVINA, M.S., KOROBEINIKOVA, O.A., LIZUNOV, A.A., MAXIMOV, V.V., MURAKHTIN, S.V., *et al.* . 2015*a* Progress in mirror-based fusion neutron source development. *Materials* **8** (12), 8452–8459.

ANIKEEV, A.V., BAGRYANSKY, P.A., ZAITSEV, K.V., KOROBEINIKOVA, O.A., MURAKHTIN, S.V., SKOVORODIN, D.I. & YUROV, D.V. 2015*b* Energy spectrum of longitudinal ion losses in the GDT facility under development of Alfvén ion-cyclotron instability. *Plasma Phys. Rep*. **41**, 773–782.

BAGRYANSKY, P.A., ANIKEEV, A.V., BEKLEMISHEV, A.D., DONIN, A.S., IVANOV, A.A., KORZHAVINA, M.S., KOVALENKO, YU.V., KRUGLYAKOV, E.P., LIZUNOV, A.A., MAXIMOV, V.V., *et al.* 2011 Confinement of hot ion plasma with $\beta = 0.6$ in the gas dynamic trap. *Fusion Sci. Technol*. **59** (1T), 31–35.

BAGRYANSKY, P.A., CHEN, Z., KOTELNIKOV, I.A., YAKOVLEV, D.V., PRIKHODKO, V.V., ZENG, Q., BAI, Y., YU, J., IVANOV, A.A. & WU, Y. 2020 Development strategy for steady-state fusion volumetric neutron source based on the gas-dynamic trap. *Nucl. Fusion* **60** (3), 036005.

BEKLEMISHEV, A.D., BAGRYANSKY, P.A., CHASCHIN, M.S. & SOLDATKINA, E.I. 2010 Vortex confinement of plasmas in symmetric mirror traps. *Fusion Sci. Technol*. **57** (4), 351–360.

BERZINS, L.V. & CASPER, T.A. 1987 Ion microinstability at the outer sloshing-ion turning point of the tandem mirror experiment upgrade (TMX-U). *Phys. Rev. Lett*. **59** (13), 1428.

CHEN, Z., BAGRYANSKY, P., ZENG, Q., ZOU, J., ZHANG, K., WANG, Z., JIA, J., ZHANG, S., DONG, L., ZHA, X., *et al.* 2022 Summary of the 3rd International Workshop on Gas-Dynamic Trap based Fusion Neutron Source (GDT-FNS). *Nucl. Fusion* **62** (6), 067001.

CHERNOSHTANOV, I.S. 2016 Effect of alfvén ion-cyclotron instability on ion dynamic in an axisymmetric mirror trap. *AIP Conference Proceedings* **1771**, 040009.

CHERNOSHTANOV, I.S. 2018 Ion losses induced by Alfvén ion-cyclotron instability in mirror machine with skew neutral beam injection. In *Journal of Physics: Conference Series*, vol. 1125, p. 012007. IOP Publishing.

COENSGEN, F.H., CUMMINS, W.F., LOGAN, B.G., MOLVIK, A.W., NEXSEN, W.E., SIMONEN, T.C., STALLARD, B.W. & TURNER, W.C. 1975 Stabilization of a neutral-beam—sustained, mirror-confined plasma. *Phys. Rev. Lett*. **35** (22), 1501.

FERRARO, R.D., LITTLEJOHN, R.G., SANUKI, H. & FRIED, B.D. 1987 Nonlocal effects on the drift cyclotron loss cone dispersion relation in cylindrical geometry. *Phys. Fluids* **30** (4), 1115–1122.

FERRON, J.R. & WONG, A.Y. 1984 The dependence of the drift cyclotron loss cone instability on the radial density gradient. *Phys. Fluids* **27** (5), 1287–1300.

IVANOV, A.A. & PRIKHODKO, V.V. 2017 Gas dynamic trap: experimental results and future prospects. *Phys.-Usp*. **60** (5), 509.

KANAEV, B.I. 1979 Stabilization of drift loss-cone instability (DCI) by addition of cold ions. *Nucl. Fusion* **19** (3), 347.

KOEPKE, M., MCCARRICK, M.J., MAJESKI, R.P. & ELLIS, R.F. 1986 Three-dimensional mode structure of the drift cyclotron loss-cone instability in a mirror trap. *Phys. Fluids* **29** (10), 3439–3444.

KOTELNIKOV, I.A. & CHERNOSHTANOV, I.S. 2018 Isotopic effect in microstability of electrostatic oscillations in magnetic mirror traps. *Phys. Plasmas* **25** (8), 082501.

KOTELNIKOV, I.A., CHERNOSHTANOV, I.S. & PRIKHODKO, V.V. 2017 Electrostatic instabilities in a mirror trap revisited. *Phys. Plasmas* **24** (12), 122512.

LEIKIND, B.J., ZWI, H., DIMONTE, G. & WONG, A.Y. 1985 Spatial localization of bursts of the drift cyclotron loss cone instability. *Phys. Fluids* **28** (5), 1219–1221.

LIZUNOV, A.A., DEN HARTOG, D.J., DONIN, A.S., IVANOV, A.A. & PRIKHODKO, V.V. 2011 Note: multi-point measurement of |B| in the gas-dynamic trap with a spectral motional Stark effect diagnostic. *Rev. Sci. Instrum*. **82** (8), 086105.

LIZUNOV, A., BERBASOVA, T., KHILCHENKO, A., KVASHNIN, A., PURYGA, E., SANDOMIRSKY, A. & ZUBAREV, P. 2023 High resolution Thomson scattering diagnostic for measurements of radial profiles of electron temperature and density in the gas dynamic trap. *Rev. Sci. Instrum*. **94** (3), 033509.

LVOVSKIY, A.V. & SOLOMAKHIN, A.L. 2011 Line plasma density measurement in the gas dynamic trap with dispersion interferometer. *Fusion Sci. Technol*. **59** (1T), 298–300.

MIRNOV, V.V. & RIUTOV, D.D. 1979 Linear gasdynamic system for plasma confinement. *Tech. Phys. Lett*. **5**, 279.

POST, R.F. 1987 The magnetic mirror approach to fusion. *Nucl. Fusion* **27** (10), 1579–1739.

POST, R.F. & ROSENBLUTH, M.N. 1966 Electrostatic instabilities in finite mirror-confined plasmas. *Phys. Fluids* **9** (4), 730–749.

SCARGLE, J.D. 1982 Studies in astronomical time series analysis. II-statistical aspects of spectral analysis of unevenly spaced data. *Astrophys. J*. **263**, 835–853.

SHALASHOV, A.G., GOSPODCHIKOV, E.D., KHUSAINOV, T.A., LUBYAKO, L.V., SOLOMAKHIN, A.L. & YAKOVLEV, D.V. 2022 First results of collective Thomson scattering diagnostic of fast ions at the GDT open magnetic trap. *Phys. Plasmas* **29** (8), 080702.

SIMONEN, T.C. 1976 Measurements of ion cyclotron instability characteristics in a mirror-confined plasma. *Phys. Fluids* **19** (9), 1365–1370.

SIMONEN, T.C., ANIKEEV, A., BAGRYANSKY, P., BEKLEMISHEV, A., IVANOV, A., LIZUNOV, A., MAXIMOV, V., PRIKHODKO, V. & TSIDULKO, YU. 2010 High beta experiments in the GDT axisymmetric magnetic mirror. *J. Fusion Energy* **29**, 558–560.

SOLDATKINA, E.I., MAXIMOV, V.V., PRIKHODKO, V.V., SAVKIN, V.YA., SKOVORODIN, D.I., YAKOVLEV, D.V. & BAGRYANSKY, P.A. 2020 Measurements of axial energy loss from magnetic mirror trap. *Nucl. Fusion* **60** (8), 086009.

TANG, W.M., PEARLSTEIN, L.D. & BERK, H.L. 1972 Finite beta stabilization of the drift-cone instability. *Phys. Fluids* **15** (6), 1153–1155.

TSANG, K.T. & SMITH, G.R. 1987 Stability of alfvén ion-cyclotron modes with finite perpendicular wavenumber. *Phys. Fluids* **30** (5), 1362–1366.

TURNER, W.C. 1977 Electrostatic ion cyclotron waves and ion energy diffusion in a mirror machine. *J. Phys*. **38**, C6–121.

TURNER, W.C., POWERS, E.J. & SIMONEN, T.C. 1977 Properties of electrostatic ion-cyclotron waves in a mirror machine. *Phys. Rev. Lett*. **39**, 1087–1091.

WATSON, D.C. 1980 Alfvén-ion-cyclotron instability in mirror machines. *Phys. Fluids* **23** (12), 2485–2492.

YUROV, D.V. & PRIKHOD'KO, V.V. 2014 Hybrid systems for transuranic waste transmutation in nuclear power reactors: state of the art and future prospects. *Phys.-Usp*. **57** (11), 1118.

YUROV, D.V. & PRIKHODKO, V.V. 2016 Optimization of a mirror-based neutron source using differential evolution algorithm. *Nucl. Fusion* **56** (12), 126003.

ZAYTSEV, K.V., ANIKEEV, A.V., BAGRYANSKY, P.A., DONIN, A.S., KOROBEINIKOVA, O.A., KORZHAVINA, M.S., KOVALENKO, YU.V., LIZUNOV, A.A., MAXIMOV, V.V., PINZHENIN, E.I., *et al.* 2014 Kinetic instability observations in the Gas Dynamic Trap. *Phys. Scr*. **2014** (T161), 014004.

ZAYTSEV, K.V., ANIKEEV, A.V., BAGRYANSKY, P.A., DONIN, A.S., KOVALENKO, YU.V., KORZHAVINA, M.S., LIZUNOV, A.A., LOZHKINA, A.N., MAXIMOV, V.V., PINZHENIN, E.I., *et al.* 2013 Magnetic measurements at the GDT facility. *Fusion Sci. Technol*. **63** (1T), 346–348.